Using the 546 nm green line emission of mercury to determine its hyperfine structure

Jade Salisbury and *Samuel Novak*

10867885 and *10832664*

Department of Physics and Astronomy

University of Manchester

Second year laboratory report

February 2023

Abstract

Using emission spectroscopy of the 546 nm green line, the hyperfine structure of naturally occurring mercury was calculated. The $7^3S_1 \rightarrow 6^3P_2$ transition, that produces a photon of approximately 546 nm, is split into multiple possible transitions due to the interaction between the orbital angular momentum and spin of the valence electrons and the spin of the nucleus. The measured transitions agreed with the calculated theoretical transitions to within 2 standard deviations. The free spectral range of the diffraction pattern was found to be (34.77 ± 2.74) GHz which agrees with the theoretical value of (37.50 ± 0.09) GHz. The main source of error was found to be systematic and arised due to the Doppler broadening of the emission lines.

1 Introduction

The modern model of the atom consists of a nucleus at the centre with electrons surrounding at designated orbitals. The outermost electrons, known as valence electrons, are able to transition between states of higher and lower energies and release photons as a result (fluorescence). Thus, measuring the emission from a given element produces a spectrum that can be analysed in order to calculate the electronic structure. Interactions between the spins of the nucleus and electrons create small energy shifts that increase the number of possible transitions, known as the hyperfine structure. This experiment focuses on measuring the emission from a lamp containing naturally occurring mercury. Therefore, it is a combination of all the stable isotopes in proportions relative to the abundance of each isotope. The emission line of interest occurs due to the $7^3S_1 \rightarrow 6^3P_2$ transition with the corresponding fine and hyperfine splitting. Mass shift of isotopes with no nuclear spin is also apparent and is explained later in the theory section.

2 Theory

Mercury has 80 electrons and protons and forms over 35 isotopes. Seven of these isotopes are stable and are shown in table 1 with the corresponding natural abundances. In the ground state, there are two valence electrons located in the outermost orbital: n=6, where n is the principal quantum number. The remaining 78 are distributed in the inner orbitals (n=1 to n=5) and do not affect the excitation/emission process.

Table 1: Isotopes of Hg with corresponding relative abundances [1].

Hg isotope	Relative abundance
^{196}Hg	0.16%
^{198}Hg	10.0%
^{199}Hg	16.9%
^{200}Hg	23.1%
^{201}Hg	13.2%
^{202}Hg	29.7%
^{204}Hg	6.83%

The spin and orbital angular momentum of an electron interact through a process known as LS coupling. If the assumption is made that, for individual electrons, the spin (s_i) and orbital angular momentum (l_i) all couple together independently, then the final interaction is given only by the total electron spin (**S**) and total orbital angular momentum (**L**). **S** and **L** are the linear summation of the s_i and l_i values. The total angular momentum (**J**) is then found using the vectorial summation given by the equation

$$\mathbf{J} = \mathbf{L} + \mathbf{S}. \tag{1}$$

J has a magnitude ranging from **L** + **S** to |**L** – **S**| in integer steps. Variations in the value of **J** result in relative changes in energy (splitting) of the excited states. This is known as the fine structure splitting and it is a result of the Pauli exclusion principle. It states that two or more fermions cannot occupy the same quantum state within a quantum system [2]. Electrons of equal spin cannot occupy the same state and are on average more separated than electrons in the same state but with opposite spins. This results in a reduction in the Coulomb force experienced by the electrons and therefore a change in energy.

In order to minimise the energy of the mercury atom, the inner electrons form pairs with opposite spin ($s_i = \pm\frac{1}{2}$ in units of $\hbar$) and their combined orbital angular momentum is zero. Therefore, the total angular momentum of the atom is determined exclusively by the outer electrons.

A further splitting of the energy states arises due to the effect of the nuclear spin. Like electrons, nucleons have spin values (i_μ) of $\frac{1}{2}$ and minimise energy by pairing up such that the total spin (**I**) is zero. For isotopes of with an odd number of nucleons, it is not possible for every nucleon to form a pair with another. This results in an overall spin to the nucleus. For mercury, the isotopes ^{199}Hg and ^{201}Hg have non-zero nuclear spin with nuclear spins of $\mathbf{I} = \frac{1}{2}$ and $\mathbf{I} = \frac{3}{2}$ respectively.

The nuclear spin contributes to the overall angular momentum F according to the equation

$$\mathbf{F} = \mathbf{J} + \mathbf{I} \tag{2}$$

where **F** can have a magnitude ranging from $\mathbf{F} = \mathbf{J} + \mathbf{I}$ to |**J** – **I**| in integer intervals. Variations in **F** lead to smaller splittings of the energy levels than the fine structure and is known as the hyperfine structure. The energy levels and possible transitions for ^{199}Hg and ^{201}Hg are shown in figure 1 with the corresponding **F** values for each energy state.

The energy shift due to this is approximated as a first order perturbation to the Hamiltonian of the system. The interaction Hamiltonian, H^{HFS}, is given by the equation [3]

$$H^{HFS} = a^{HF}\frac{\mathbf{I}\cdot\mathbf{J}}{\hbar^2} + b^{HF}\left(\frac{3\left(\frac{\mathbf{I}\cdot\mathbf{J}}{\hbar^2}\right)^2 + 3\left(\frac{\mathbf{I}\cdot\mathbf{J}}{2\hbar^2}\right) - \left(\frac{\mathbf{I}^2\mathbf{J}^2}{\hbar^4}\right)}{2I(2I-1)J(2J-1)}\right) \tag{3}$$

where a^{HF} is the magnetic dipole constant and b^{HF} is the electric quadrupole constant. $\mathbf{I}\cdot\mathbf{J}$ is the dot product of **I** and **J** and is given by the equation

$$\mathbf{I}\cdot\mathbf{J} = \frac{1}{2}\left(\mathbf{F}^2 - \mathbf{I}^2 - \mathbf{J}^2\right). \tag{4}$$

For the isotopes of mercury that have no net nuclear spin, the energy of the isotopic states also have small changes due to the mass (isotope) shift. This arises due to the different structure of

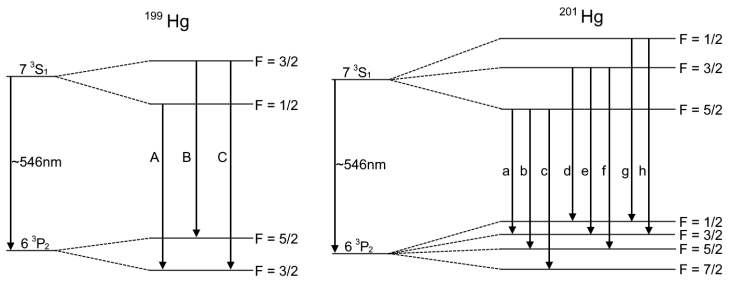

Figure 1: The hyperfine energy level diagrams for the isotopes with non-zero spin: ^{199}Hg and ^{201}Hg. The states on the left side of each diagram show the energy levels before hyperfine splitting and the effect of splitting are shown on the right. The possible transitions are shown by vertical arrows that are labelled A-C for ^{199}Hg and a-h for ^{201}Hg. Possible transitions occur if $\Delta\mathbf{F}$ is equal to $\pm 1, 0$.

the nuclei as the different distributions of nucleons change with each isotope. As a result, the Coulomb interaction between the protons and orbiting electrons is changed, resulting in further energy level splitting.

The energy of the emitted photon is equal to the energy difference between the two states. The frequency of the photon can be found using the Planck-Einstein relation [4]

$$\Delta E = h\nu \tag{5}$$

where ΔE is the difference in energy, h is Planck's constant and ν is the frequency. The difference in frequencies of photons emitted due to the hyperfine splitting leads to constructive and destructive interference after passing through the etalon, as explained in the next section.

3 Experimental approach

The equipment is set up as shown in figure 2. Photons are emitted from the mercury particles within the Hg lamp which are travelling in all directions. This is shown on the left of figure 2. The rays become quasi-collimated as they pass through the 35 mm lens, as the lens refracts the rays such that they are diverging by a small angle. The green 546 nm filter decreases the range of wavelengths of light that interact with the camera lens, decreasing the difficulty of discerning the hyperfine line emission structure. The adjustable aperture restricts the intensity of light that enters the camera lens. The clearest results were achieved when the aperture was nearly closed, and the exposure of the camera was long, increasing the sharpness of the images as they consist of rays only travelling parallel to the components.

The light arrives at the etalon. An etalon (Fabry-Pérot interferometer) is a precisely manufactured device consisting of two near perfectly parallel reflective surfaces. This means that the rays

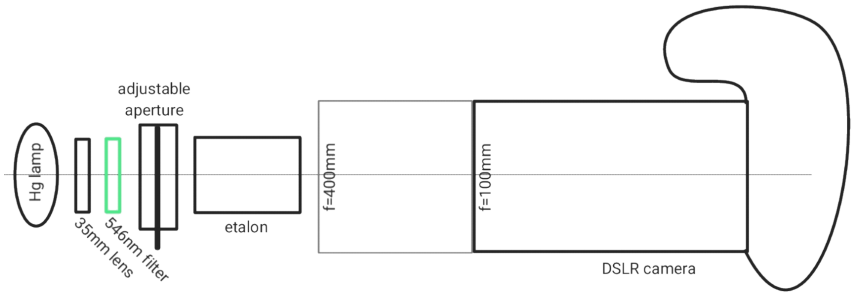

Figure 2: A diagram detailing the order in which the components were setup for the experiment. Consisting of: a mercury lamp, a 35 mm lens, a 546 nm green filter, an adjustable aperture, the etalon and a digital single-lens reflex (DSLR) camera with a lens of focal length 100 - 400 mm (fixed at 400 mm in this experiment). In order to remove any unwanted light rays, the setup is contained within a covered box.

exit parallel to one another, as shown on figure 3, with minimal scattering losses. Distance d on the etalon for this experiment had a value of (4.00 ± 0.01)mm, leading to a very small source of error. The intensity of the interference pattern formed on the sensor of the camera can be described by the equation

$$\frac{I_{out}}{I_0} = \frac{1}{1 + F_R \sin^2 \phi} \tag{6}$$

where the phase shift ϕ and F_R are given by the equations

$$F_R = \frac{4R}{(1-R)^2} \tag{7}$$

$$\phi = \frac{2\pi d}{\lambda} \cos\theta \tag{8}$$

where R is the reflectivity, given by the equation [5] $R = \sqrt{r_1 r_2}$ and θ is the angle from which the light emerges from the etalon's normal. The transmission coefficients $t_{1,2}$ similarly form T and together the equation $T + R = 1$ holds. $R = 0.93$ for this etalon. From the above equations it is derived that maxima occur when the equation

$$2d \cos\theta = n\lambda \tag{9}$$

holds, where n is an integer representing the *order* of the maxima, imaged in the focal plane of the camera as if they were observed from infinity. If measuring to a high resolution, handling the results in terms of frequency shifts rather than wavelength shifts is preferred. The free spectral range (FSR) determines the frequency distance between repeating fringes and is given by the equation

$$FSR = \Delta\nu_{FSR} = \frac{c}{2d} \tag{10}$$

where c is the speed of light and d is the distance between the mirrors of the etalon. The etalon used in this experiment gives an FSR value of (37.50 ± 0.09)GHz.

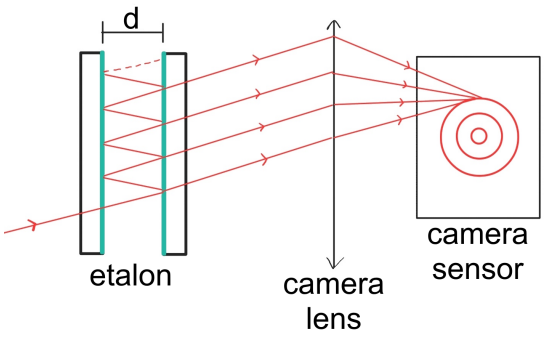

Figure 3: A diagram to show how the light rays (red) that enter the etalon on the left are reflected within the device. The green lines represent the highly reflective surfaces, with the left and right surfaces having reflectivity and transmission coefficients of $r_{1,2}$ and $t_{1,2}$ respectively. With each reflection, a portion of light, determined by $t_{1,2}$, is transmitted through the etalon. These are converged by the camera lens forming an interference pattern with circular symmetry. Note that only the transmitted light rays of interest are shown.

The radial position of the maxima depends on the wavelength of light and small changes in wavelengths due to the hyperfine splitting occur as separate maxima that directly relate to each transition. The average intensity around the whole fringe (2π radians) was computed in order to convert the circular diffraction pattern to a graph of intensity against frequency. Gaussian distributions were used to model the diffraction pattern such that the centre of each Gaussian represented the equivalent frequency of each maxima.

The DSLR camera has multiple variables that can be customised to maximise the sharpness and visibility of the diffraction pattern. Three of interest include the aperture, ISO (International Organization for Standardization) and shutter speed (equivalent to the exposure time). The best results were found to be given when the aperture was f/8, a shutter speed of 30s and an ISO of 1250.

4 Results

The Gaussian curves in figure 4 are predicted to be the best fits through an algorithm. By plotting the frequency shifts found in theory and aligning them, the highest and most central peak is the ^{198}Hg reference line. To confirm this: the $7^3S_1 \rightarrow 6^3P_2$ transition in ^{198}Hg is known to be surrounded by other transitions that will be combined by broadening *and* has a high abundance. The frequency shifts to each of the other peaks can be calculated from this and then matched to each transition or set of transitions (when they are too close to be individually discerned). Table 2 shows the result of this.

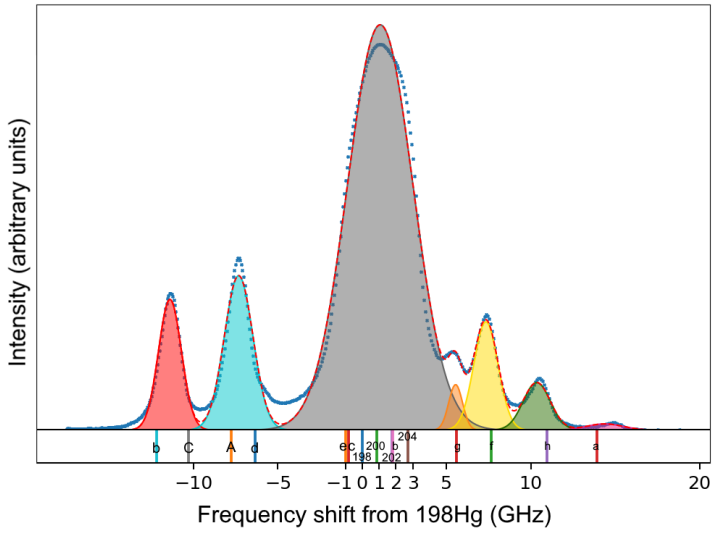

Figure 4: Frequency measures, (blue dots) with associated Gaussian curve predictions (red line). Underneath are the labelled associated transitions and their distance from the reference line (same scale). Gaussians are labelled linearlly from left to right.

Table 2: Fitted Gaussians and corresponding frequency shifts from ^{198}Hg.

#	Frequency shift from ^{198}Hg (GHz)	Associated transition(s)*	Theoretical Frequency Shift (GHz)
1	-12.50 ± 2.06	C, b	24.47, -0.83,
2	-8.42 ± 2.12	A, d	-7.78, -6.36
3	0 ± 1.94	^{204}Hg, ^{202}Hg, ^{200}Hg, ^{198}Hg, B, c, e	0
4	4.49 ± 1.99	g	5.57
5	6.29 ± 2.07	f	7.64
6	9.32 ± 2.10	h	10.95
7	-21.41 ± 2.22	a	-20.84

* Associated transitions refers to the transitions which lie close enough to this peak in the line emission such that they cannot be resolved into their own peak. The zero point has been taken to be the tallest Gaussian and the expected ^{198}Hg line.

Uncertainty in this experiment comes from several sources. One systematic source of uncertainty is due to the quantum mechanical effect explained in Heisenberg's uncertainty principle, giving lines a Lorentzian line profile [6]. The shapes are widened towards a Gaussian shape as a result of Doppler broadening from the kinetic movement of the mercury particles of a temperature $\approx$ 1000K. These sources of errors compound and form the Gaussian shapes which can be used to find the total combined uncertainty on each of their frequencies. The uncertainties on each of the frequency shifts are calculated using the combined uncertainty coming from the equation

$$\sigma = \frac{1}{2\sqrt{2\ln 2}} \Delta f_{FWHM} \tag{11}$$

where Δf_{FWHM} is the full width of the Gaussian at half its maximum, and σ is the standard deviation. Multiplying the error on the reference line by $\sqrt{2}$ and finding the frequency shift between repeating patterns gave a value of free spectral range to be $FSR = (34.77 \pm 2.74)$ GHz. Having FSR allows the association of transitions to the leftmost and rightmost Gaussians as they correspond to transitions from the previous and next order of fringes.

Results found corresponded well with transition frequency shifts obtained from theory. The most accurate to those predicted by theory fell within a standard deviation, and those that did not, fell within two standard deviations. The main source of error for any given value was Doppler broadening, however the merging of multiple transitions around ^{198}Hg meant that the standard deviation on the Gaussian for the reference line was larger than any other, and this uncertainty was used in the error on every shift from the reference line. To reduce uncertainty, the mercury could be cooled enough to reduce Doppler broadening such that transitions near the reference line can be individually resolved, reducing uncertainty on every frequency shift.

5 Conclusions

The results for this experiment clearly demonstrate the presence of the hyperfine structure in the mercury atom. The results corresponded well with predicted frequency shifts, all falling within 2 standard deviations of the theoretical values. A free spectral range of (34.77 ± 2.74) GHz was found through the repeating frequency pattern.

References

[1] J. Blum *et al.*, "Mercury isotopes identify near-surface marine mercury in deep-sea trench biota," *Proceedings of the National Academy of Sciences of the United States of America*, vol. 117, 2020.

[2] W. Pauli, "Über den Zusammenhang des Abschlusses der Elektronengruppen im Atom mit der Komplexstruktur der Spektren," *Zeitschrift für Physik*, vol. 31, pp. 765–783, 1925.

[3] B. H. Bransden and C. J. Joachain, *Physics of Atoms and Molecules*. 2003.

[4] A. Einstein, "Zur Elektrodynamik bewegter Körper," *Annalen der Physik*, vol. 322, pp. 891–921, 1905.

[5] F. A. Jenkins and H. E. White, *Fundamentals of Physical Optics*. 1950.

[6] *Radiative Transitions between Discrete States in Atomic Systems*. John Wiley Sons, Ltd, 1997.